Supplemental Data

Functional Effects of a Neuromelanin Analog on Dopaminergic Neurons in 3D Cell Culture

Will Collins [1, 2], Nicolas Rouleau [2, 3], Mattia Bonzanni [2, 3], Kevin Kapner [2], Alex Jeremiah [2], Chuang Du [2], Emmanuel N Pothos [1], David L Kaplan [2,3,]*

(1) Department of Pharmacology & Experimental. Therapeutics, Sackler School of Graduate Biomedical Sciences, Tufts University School of Medicine, Tufts University, Boston MA, 02111

(2) Department of Biomedical Engineering, 4 Colby St. Tufts University, Medford MA, 02155

(3) Tufts Allen Discovery Center, 200 College Ave. Tufts University Medford MA, 02155

(*) Corresponding Author: David.Kaplan@Tufts.edu

Pages: 12

Figures: 6

Tables: 4

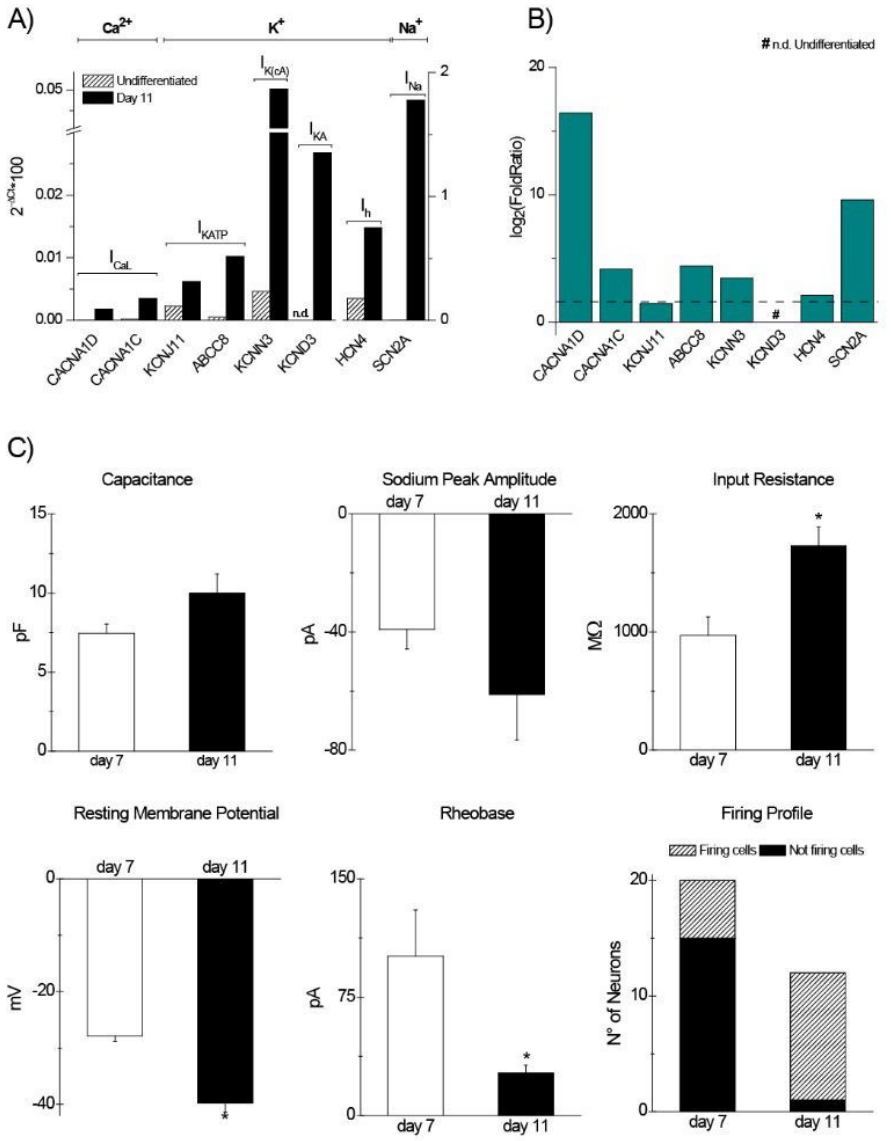

	Day 7			Day 11		
Parameter	Sample size	Mean	S.E.M.	Sample size	Mean	S.E.M.
Capacitance (pF)	19	7.5	0.6	11	10.0	1.2
Sodium peak amplitude (pA)	10	-39.1	6.6	8	-61.1	15.5
Input Resistance (MΩ)	11	970.4	156.5	10	1728.2*	158.0
Resting Membrane potential (mV)	20	-27.9	0.9	11	-39.8*	1.5
Rheobase (pA)	5	101.0	29.2	8	26.9*	5.0

Supplemental Figure 1. Comparison of Expression Profile and Functional Features of LUHMES Differentiation A-B) The qPCR data compares the undifferentiated and day 11 differentiation conditions. mRNA expression of ion channels and relative fold increase (dash line is the threshold set as Fold Ratio=2) (N=1). **C)** The electrophysiological data compares the day 7 and day 11 of differentiation conditions. Electrophysiological parameters recorded with the patch clamp technique. * $p<0.05$ using Student's T-Test.

Along with chemical communication, mature neurons generate and dynamically integrate electrical signals. To acquire a functional electrophysiological phenotype over the differentiation process of LUHMES progenitors to the dopaminergic state, cells express ion channels and accessory proteins. To investigate this maturation, we

compared by RT-qPCR the mRNA expression levels of 8 ion channels that are the dominant molecular determinants of the main neuronal ionic currents (n=1). After eleven 11 days of differentiation (Supplemental 1A), all subunits except KCND3 increased by 2-fold or more expression in comparison to the undifferentiated condition (controls) (Supplemental 1B). In line with the gene expression data, we observed a maturation of the electrical properties of LUHMES cells (day 7 vs day 11 of differentiation; Supplemental 2C). The input resistance ($p<0.05$) increased as the cells matured over time, concomitant with significant hyperpolarization of the resting membrane potential and a decrease of the rheobase (injected current necessary to induce the action potential) ($p<0.05$). We did not observe any significant cell size change, as measured by capacitance. Taken together, these data indicate molecular and functional maturation of LUHMES dopaminergic neurons.

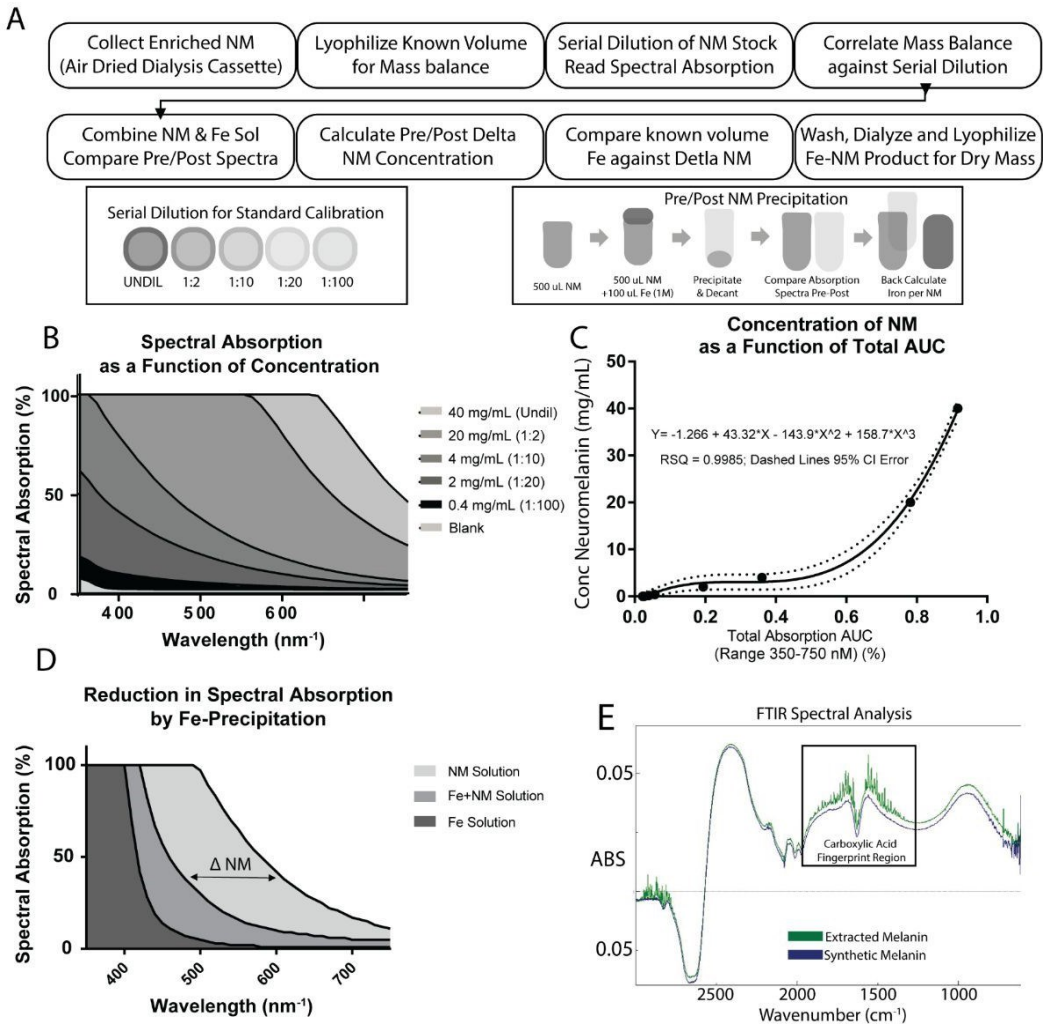

Supplemental Figure 2. Methods for Spectral Calibration of NM solution, Quantification of Fe-NM Precipitation A. Aq. Melanin solution was enriched by air drying in dialysis cassettes and a known volume (10 mL) was frozen and lyophilized for mass balance. The remaining NM solution was diluted in the following manner (1) 1:2 (2) 1:10 (3) 1:20 and (4) 1:100 to establish a calibration curve and read by spectral absorption profile. To define the stoichiometric ratio of Fe to NM, a 500 uL solution of NM was combined with 100 uL of Fe solution (1M) and the pre/post spectral area under the curve (AUC) values were compared. The delta was used to estimate the NM precipitated. **B.** The AUC values allow for concentration estimation and follow a hyperbolic function **C.** In estimating the concentration of NM against its total AUC, estimation followed a third order polynomial. **D.** Calculation of the ΔNM is expressed as the difference in area between pre and post Fe precipitation expressed as ΔAUC for the calibration curve **E.** The integrity of NM carboxylic acid groups can be assessed following processing with Fourier Transform IR (FTIR) analysis between 1500-1000 cm^{-1}.

The technique for spectral determination of NM allows indirect quantification of the amount of NM against a known concentration of Fe before precipitation. While the reduction in spectral absorption is not as exact as chromatography, it allows quantification of Fe-NM precipitation. Results suggest a stoichiometric ratio of 2 NM to 1 Fe in precipitation.

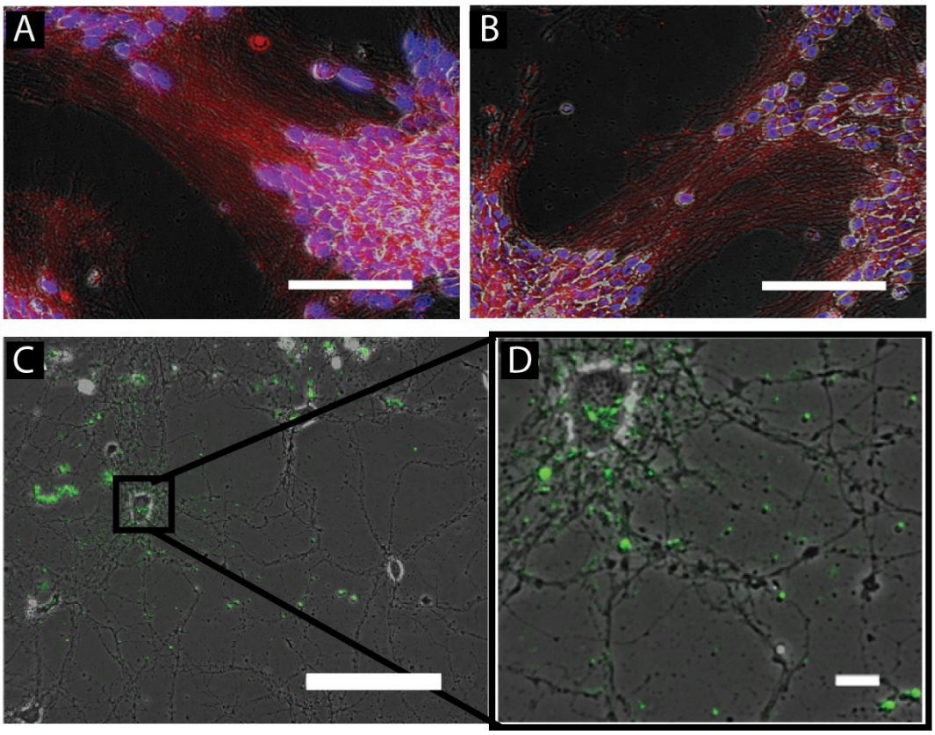

Supplemental Figure 3. Immunostaining Evidence of Dopaminergic Phenotype. A.B. The presence of tyrosine hydroxylase (TH –Red; DAPI-Blue; scale 100 uM) and dopamine receptor D2 (DRD2-Red; DAPI -Blue; scale 100 uM) were observed in the D-7 differentiated LUHMES cells, validating the dopaminergic phenotype following one week in culture. D.C. Phen-green, which stains free iron demonstrates a similar punctate staining (Phen-Green – Green; scale 100 uM and 10 uM).

Dopaminergic neurons rely on tyrosine hydroxylase (TH) as the primary means of producing the neurotransmitter dopamine. TH requires iron as a metal catalyst to perform its function in converting L-DOPA to dopamine. DRD2 receptors suggest that the cells are additionally capable of sensing neurotransmitters in solution. Furthermore, neural cultures that exhibit dendritic beading also stain positive for Phen-Green as well in punctate areas, suggesting free metals may be present.

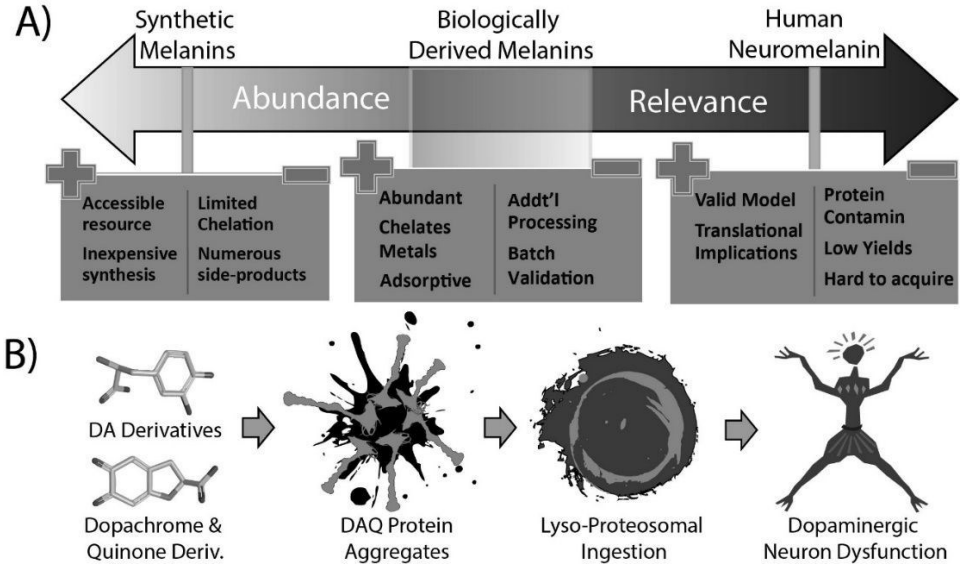

Supplemental Figure 4. Schematic of Challenges of Neuromelanin Availability and Parkinson's Disease Relevance. A. Forming synthetic melanins is a chemical process and the product lacks the structural integrity of extracted biological melanins. However, these biologically extracted melanins are labor/resource intensive to acquire and yield poor outcomes, especially in the case of NM. For this reason, a biomaterial was pursued which possesses properties of chelation while not identical to endogenous NM. **B.** Dopamine and its derivatives have been noted to be especially chemically reactive and form quinone side-products (dopaquinones - DAQ) or internally rearrange to form chromophores (dopachrome). Unless these reactive side products are integrated into a NM structure, DAQ can integrate with proteins and form aggregates which are then consumed by either the lysosome or proteasome resulting in neural dysfunction as cells cannot clear these aggregates commonly known as Lewy bodies in clinical literature.

Information concerning the effects of NM on microglial activity is available in the literature which describes the antagonistic relationship between insoluble protein aggregates and neuro-inflammation. Microglia release a cascade of inflammatory cytokines and engage in 'respiratory burst' events in which release of nitric oxide, peroxides and other free radicals occur. These reactive nitrogen species (RNS) and reactive oxygen species (ROS) are capable of further interaction to form 'superoxide radicals' which are detrimental to the proteome, resulting in irreparable damage (Beckman et al., 1996). The DAQ quinone derivatives exacerbate this problem by chemically stabilizing existing protein interactions, contributing to protein insolubility and DA neuron death (Sulzer, 2007), while inciting the microglia to cause further neuroinflammation (Gao et al., 2002). This figure was modelled after the work of Zucca et al., 2014.

Literature:

(1) Beckman, Joseph S., and Willem H. Koppenol. "Nitric oxide, superoxide, and peroxynitrite: the good, the bad, and ugly." American Journal of Physiology-Cell Physiology 271.5 (1996): C1424-C1437

(2) Sulzer, David. "Multiple hit hypotheses for dopamine neuron loss in Parkinson's disease." Trends in neurosciences 30.5 (2007): 244-250

(3) Gao, Hui-Ming, et al. "Distinct role for microglia in rotenone-induced degeneration of dopaminergic neurons." Journal of Neuroscience 22.3 (2002): 782-790.

(4) Zucca, Fabio A., et al. "Neuromelanin of the human substantia nigra: an update." Neurotoxicity research 25.1 (2014): 13-23.

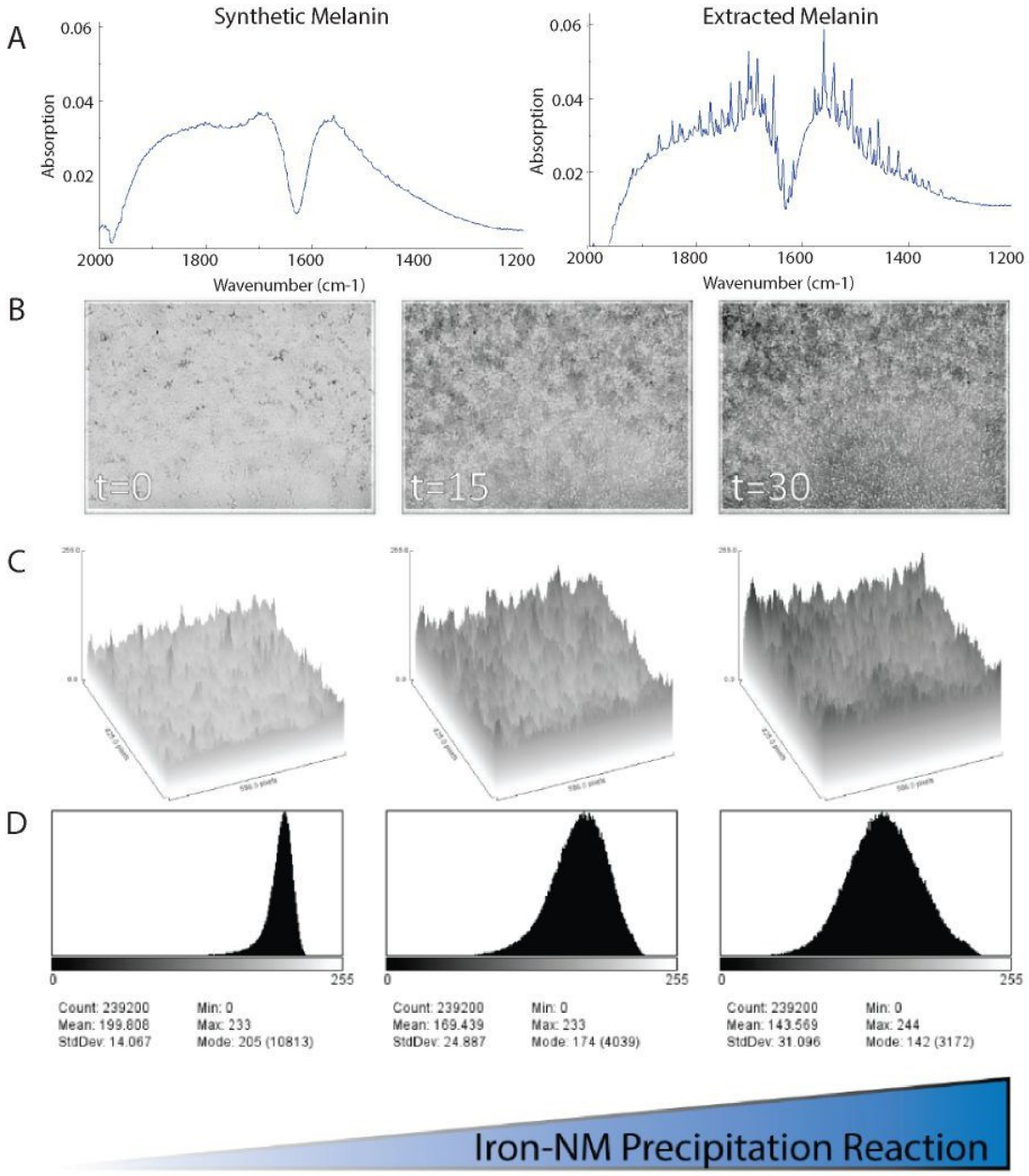

Supplemental Figure 5. Comparison of Synthetic and Extracted Melanin and Time course of Precipitation. **A.** Comparison of FTIR spectral profiles for comparison between the synthetic and extracted melanins in the spectral range of 2000-1200 cm^{-1}. This suggests that there is limited presence of carboxyl groups in the synthetic melanin which would reduce capability of metal chelation. **B.** A time-course of the metal precipitation reaction with iron (i.e. extracted melanin) is shown in black and white (frames t=0; t=15 and t=30 min). **C.** 3D rendering of this precipitation in B is illustrated over the course of precipitation for spectral analysis. **D.** The rate of precipitation was qualified by creating a histogram over collected video-frames to allow for kinetic evaluation by evaluation of the Area Under the Curve (AUC) values.

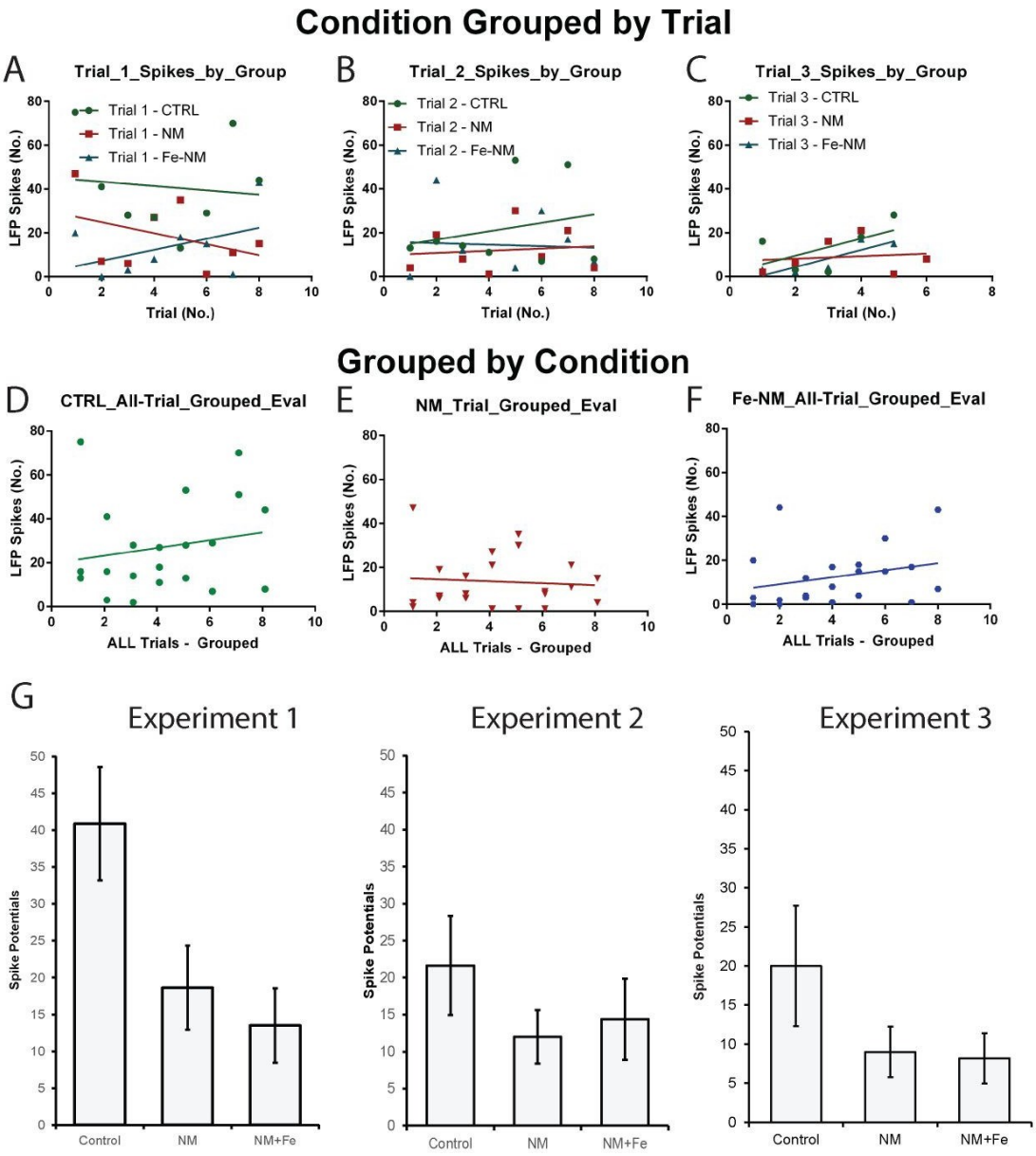

Supplemental Figure 6. Experimental Trial and Experimental Condition Groupings. Results shown in Figure 3 of the main text depict the aggregation of three experimental trials in which individual conditions are color mapped and approximated to ensure that no temporal effects have occurred (i.e. condition specific trending over duration of experiment). **A**. The collective LFP results of Trial 1 **B**. The collective LFP results of Trial 2 **C**. The collective LFP results of Trial 3 (All color coded by experimental condition against the trial order number). **D.** Combined results of all control conditions against trial number **E.** Combined results of all NM-sim conditions against trial number **F.** Combined results of all Fe-NM-sim conditions against trial number. G. All trials can be seen individually error bars are expressed as $\pm$ SEM and each experimental condition N=~8.

Collectively the results suggest that differences in experimental groupings replicate across multiple trials and the phenomena of reduced activity by LFP can be replicated independently. Furthermore R-squared values (RSQ) for all slope approximations were below any trend suggesting the phenomena was independent of time (i.e. generally RSQ < ~0.3). The phenomena of NM-sim effects on electrical activity can be observed across multiple experimental trials and replicates.

Gene	Full Name	Assay ID	Entrez Gene ID	UniGene
CACNA1D	calcium voltage-gated channel subunit alpha1 D	Hs00167753_m1	776	Hs.476358
CACNA1C	calcium voltage-gated channel subunit alpha1 C	Hs00167681_m1	775	Hs.118262
KCNJ11	potassium voltage-gated channel subfamily J member 11	Hs00265026_s1	3767	Hs.248141
ABCC8	ATP binding cassette subfamily C member 8	Hs01093752_m1	6833	Hs.54470
KCNN3	Potassium calcium-activated channel subfamily N mem. 3	Hs01546821_m1	3782	Hs.490765
KCND3	potassium voltage-gated channel subfamily D member 3	Hs00986860_m1	3752	Hs.666367
HCN4	hyperpolarization activated cyclic nucleotide gated ch 4	Hs00975492_m1	10021	Hs.86941
SCN2A	sodium voltage-gated channel alpha subunit 2	Hs04968321_s1	6326	Hs.93485
18S	Eukaryotic 18S rRNA - Housekeeping Gene	Hs99999901_s1	HSRRN18S	N/A

Supplemental Table 1. Primers used in qPCR. Extraction of LUHMES RNA was conducted according to the manufacturer's guidelines and reverse transcribed into cDNA. All primers were selected exon-spanning wherever possible. For further details please refer to the following: (1) UniGene https://www.ncbi.nlm.nih.gov/unigene or (2) Entrez Gene ID: https://www.ncbi.nlm.nih.gov/gene.

Use of Taqman primers were conducted according to the guidelines of the manufacturer. Where possible primers were selected to be 'exon spanning' to ensure that the RNA in questions was coding and not due to the effects of contamination with genomic DNA. The genes in the table summarize a variety of voltage gated channel related genes which have discrete effects on membrane potential and differentiation.

Literature:

(1) Xiaowei Wang, Athanasia Spandidos, Huajun Wang and Brian Seed: PrimerBank: a PCR primer database for quantitative gene expression analysis, 2012 update. Nucl. Acids Res. (2012) 40 (D1): D1144-9

Primary Antibodies				
Abbrev.	**Full Name**	**Description**	**Supplier**	**Part No.**
B3T	Beta-3-tubulin	Rabbit polyclonal to beta III Tubulin	abcam	ab18207
DRD2	Dopamine Receptor D2	Anti-Dopamine D2 Receptor antibody	abcam	ab85367
TH	Tyrosine Hydroxylase	Mouse monoclonal to Tyrosine Hydroxylase	abcam	ab129991
Secondary Antibodies				
Abbrev.	**Full Name**	**Description**	**Supplier**	**Part No.**
AF-568	AlexaFlour 568	Goat Anti-mouse & Anti-Rabbit IgG (H+L)	Thermo	A-11004
AF-488	AlexaFlour 488	Goat Anti-mouse & Anti-Rabbit IgG (H+L)	Thermo	A28175

Supplemental Table 2. Antibodies used in Immunostaining. Immunostaining was conducted individually to avoid cross reactivity with polyclonal antibodies. All staining solutions were concurrently blocked with goat serum blocking buffer to prevent off target effects.

Biomarker	Relevance	Citation
Glutathione	Line of defense against mitochondrial ROS	Lidell 2018
Peroxide	Fenton chemistry generation of free radicals	Robertson 2017
ADP/ATP Ratio	Energy deficits implicit in neuronal dysfunction and dopaminergic death	Sheng 2017
Protein Carbonylation	Irreversable protein denaturation which overwhelms the proteome	Fernandez 2017
Beta-Amyloid Conc.	Protein biomarker implicated in neurodegenerative disease	Scholz 2018

Supplemental Table 3. Relevance of Biomarkers. To elaborate on the makers in Figure 4, relevance to PD is expanded here. Bio-metals (i.e. Fe2+/Fe3+) are often undermined with regard to neurodegenerative disease as their isolation and detection can be challenging requiring specialized mass spec. techniques (i.e. inductively coupled plasma, ICP-MS) for quantitative results. However, fundamental DA related enzymes like TH often require a catalytic metal to function (Ramsey et al., 1996). Furthermore, many high energy bonds are stabilized by metals (i.e., ATP and Mg^{2+}) (Grober et al., 2015) and their abundance is effected by chelation (i.e., by NM-sim) and cell metabolism would be biased.

Literature:

(1) Liddell, Jeffrey R., and Anthony R. White. "Nexus between mitochondrial function, iron, copper and glutathione in Parkinson's disease." Neurochemistry international 117 (2018): 126-138

(2) Robertson, D. S. "Proposed biochemistry of Parkinson's and Alzheimer's diseases." Medical hypotheses 109 (2017): 131-138

(3) Sheng, Zu-Hang. "The interplay of axonal energy homeostasis and mitochondrial trafficking and anchoring." Trends in cell biology 27.6 (2017): 403-416

(4) Zucca, Fabio A., et al. "Interactions of iron, dopamine and neuromelanin pathways in brain aging and Parkinson's disease." Progress in neurobiology 155 (2017): 96-119

(5) Scholz, Diana, et al. "Reduced Aβ secretion by human neurons under conditions of strongly increased BACE activity." Journal of neurochemistry (2018)

(6) Ramsey, Andrew J., Patrick J. Hillas, and Paul F. Fitzpatrick. "Characterization of the active site iron in tyrosine hydroxylase redox states of the iron." Journal of Biological Chemistry 271.40 (1996): 24395-24400

(7) Gröber, Uwe, Joachim Schmidt, and Klaus Kisters. "Magnesium in prevention and therapy." Nutrients 7.9 (2015): 8199-8226

RESEARCH ARTICLES - Parkinsons 3D Modelling				
No.	CELL LINES	Scaffolding	PD Inductions	Citation
1	C6 Astrocytes PC12 Cells Human iPSC Primary DRG	3D RAFT Scaffold; Collagen Gel	MPP+	O'Rourke 2017
No.	CELL LINES	Scaffolding	PD Inductions	Citation
2	Rat primary w DA induction; H9-hESCs	Micro-TENNS (Agarose base)	N/A	Struzyna 2018
No.	CELL LINES	Scaffolding	PD Inductions	Citation
3	transgenic mice Tg(TH-EGFP) DJ76GSAT	Photolithography Silicone Wafer	MPTP	Lu, 2013
No.	CELL LINES	Scaffolding	PD Inductions	Citation
4	Sprague-Dawley Rat Pups	Organotypic Slice Culture	N/A	Daviaud, 2012
REVIEW ARTICLEs - Parkinsons 3D Modelling				
No.	Focus			Citation
1	3D neural tissue models: From spheroids to bioprinting - integration of technological advancements to supplement the drug discovery platform and challenges thereof			Zhuang, 2018
No.	Focus			Citation
2	Towards artificial tissue models: past, present, and future of 3D bioprinting - Details of printing systems and bio-inks for rapid prototyping of partial relevance to neurodegenerative disease			Arslan-Yildiz, 2016

Supplemental Table 4. Existing 3D Models of the Substantia Nigra and Parkinson's Disease. 3D models of PD and tissue engineering for the SN in efforts to treat the disease.

Literature:

(1) O'Rourke, Caitriona, et al. "Adapting tissue-engineered in vitro CNS models for high-throughput study of neurodegeneration." Journal of tissue engineering 8 (2017): 2041731417697920

(2) Struzyna, Laura A., et al. "Tissue engineered nigrostriatal pathway for treatment of Parkinson's disease." Journal of tissue engineering and regenerative medicine (2018)

(3) Lu, Xi, et al. "A microdevice platform for visualizing mitochondrial transport in aligned dopaminergic axons." Journal of neuroscience methods 209.1 (2012): 35-39

(4) Daviaud, N., et al. "Modeling nigrostriatal degeneration in organotypic cultures, a new ex vivo model of Parkinson's disease." Neuroscience 256 (2014): 10-22

(5) Zhuang, Pei, et al. "3D neural tissue models: From spheroids to bioprinting." Biomaterials 154 (2018): 113-133

(6) Arslan-Yildiz, Ahu, et al. "Towards artificial tissue models: past, present, and future of 3D bioprinting." Biofabrication 8.1 (2016): 014103.